

RESEARCH ARTICLE

10.1002/2016GC006406

Hydrostatic pressure effect on magnetic hysteresis parameters of pseudo-single-domain magnetite

Masahiko Sato^{1,2}, Yuhji Yamamoto³, Takashi Nishioka⁴, Kazuto Kodama³, Nobutatsu Mochizuki⁵, and Hideo Tsunakawa²

Key Points:

- This paper reports the first in situ magnetic hysteresis measurements of PSD magnetite under high pressure up to 1 GPa
- Pressure effect on coercivity of PSD magnetite is clearly different from those of MD and SD magnetites
- The changes in magnetic hysteresis parameters suggest that the number of lamellar domains increases with increasing pressure

Correspondence to:

M. Sato,
m.satou@aist.go.jp

Citation:

Sato, M., Y. Yamamoto, T. Nishioka, K. Kodama, N. Mochizuki, and H. Tsunakawa (2016), Hydrostatic pressure effect on magnetic hysteresis parameters of pseudo-single-domain magnetite, *Geochem. Geophys. Geosyst.*, 17, 2825–2834, doi:10.1002/2016GC006406.

Received 26 APR 2016

Accepted 21 JUN 2016

Accepted article online 23 JUN 2016

Published online 22 JUL 2016

¹Geological Survey of Japan, National Institute of Advanced Industrial Science and Technology, Tsukuba, Japan,²Department of Earth and Planetary Sciences, Tokyo Institute of Technology, Tokyo, Japan, ³Center for Advanced Marine Core Research, Kochi University, Kochi, Japan, ⁴Graduate School of Integrated Arts and Sciences, Kochi University, Kochi, Japan, ⁵Priority Organization for Innovation and Excellence, Kumamoto University, Kumamoto, Japan

Abstract This paper reports the first in situ magnetic hysteresis measurements of pseudo-single-domain (PSD) magnetite under high pressure up to 1 GPa. The magnetic hysteresis measurements of stoichiometric PSD magnetite samples under hydrostatic pressure were carried out using a piston-cylinder high-pressure cell, and the pressure dependence of the hysteresis parameters of PSD magnetite was calculated from the hysteresis curves. It was found that coercivity (B_c) increases with increasing pressure as a quadratic function up to 1 GPa by $\sim 90\%$, which is different from the pressure dependences of B_c of multidomain and single-domain magnetites. Coercivity of remanence also increases as a quadratic function, and saturation remanence (M_{rs}) increases with pressure up to 0.5 GPa by $\sim 20\%$ until reaching saturation. In contrast, saturation magnetization is constant up to 1 GPa. The approximate demagnetizing factor calculated from the ratio B_c/M_{rs} increases with increasing pressure, suggesting that the number of lamellar domains increases with increasing pressure. The number of lamellar domains and domain wall width are theoretically estimated to increase under high pressure due to the changes in magnetostriction, elastic, and magnetocrystalline anisotropy constants, and these changes in magnetic domain structure should relate to the changes in the magnetic properties of PSD magnetite.

1. Introduction

It is well known that magnetic properties of magnetic mineral change with its grain size because of the change in the magnetic domain state from fine-grained single-domain (SD) to coarse-grained multidomain (MD). Pseudo-single-domain (PSD) is an intermediate state between SD and MD, and PSD magnetite is known to frequently occur in natural deep crustal rocks [Wasilewski and Mayhew, 1992]. Hydrostatic pressure effects on magnetic parameters of magnetic minerals are fundamental information in rock magnetism and geophysical study, especially for understanding the magnetic properties of deep crustal rocks. The hydrostatic pressure effects on various magnetic minerals included in the terrestrial and extraterrestrial rocks, such as magnetite, titanomagnetite, pyrrhotite, hematite, and Fe-Ni alloy, have generated considerable recent research interest [e.g., Bezaeva et al., 2010; Gilder et al., 2002, 2004; Gilder and LeGoff, 2008; Jiang et al., 2013]. However, only a few studies have performed magnetic hysteresis measurements of magnetite under hydrostatic pressure [Carmichael, 1969; Gilder et al., 2002; Sato et al., 2014, 2015].

Carmichael [1969] measured the hydrostatic pressure dependence of coercivity (B_c) of MD magnetite sample using a high-pressure cell constructed of nonferromagnetic beryllium-copper alloy (BeCu) and a ballistic magnetometer. He reported that B_c increased with increasing pressure at a rate of $+48\%/GPa$, while the pressure dependence was ambiguous due to the large uncertainty in measurements of B_c under pressure. Gilder et al. [2002] measured alternating current (AC) susceptibility of MD and SD magnetites in a diamond anvil cell and integrated the AC susceptibility curves to calculate hysteresis loop and magnetic hysteresis parameters. In their experiment the pressure conditions in the cell were evaluated using the ruby fluorescence spectra and hydrostatic conditions were confirmed up to <3 GPa. They found no significant change in B_c of MD magnetite up to 5.6 GPa and that B_c of SD magnetite increased with increasing pressure and significant changes occurred above 1.3 GPa.

Sato *et al.* [2014] and Sato *et al.* [2015] conducted in situ hysteresis measurements of MD and SD magnetites, respectively, under hydrostatic pressure using a high-pressure apparatus for an MPMS-XL5 magnetic property measurement system (MPMS, Quantum Design). The high-pressure apparatus enables us to directly measure the magnetic hysteresis loop with high precision. The pressure dependences of B_c of MD and SD magnetites calculated from these hysteresis measurements are different: B_c of MD magnetite linearly increases with increasing pressure at a rate of +91%/GPa while that of SD magnetite is almost constant up to 1 GPa. So far, in situ hysteresis measurements of PSD magnetite have not been done and are clearly required to determine the pressure dependence of its magnetic hysteresis parameters.

This paper reports the first in situ magnetic hysteresis measurements of PSD magnetite under hydrostatic pressure up to 1 GPa using the MPMS high-pressure apparatus [Sato *et al.*, 2012]. On the basis of experimental observations, we calculate the hydrostatic pressure dependences of the magnetic hysteresis parameters of PSD magnetite, which enable us to estimate the magnetic properties of deep crustal rocks.

2. Sample

A magnetite powder sample was prepared by hand crushing a natural magnetite crystal approximately 1 cm in size (Brazil, Komuro Minerals) and sieved in an ultrasonic bath. Then the sieved powder less than $\sim 45 \mu\text{m}$ was ground in an agate motor with ethanol. The ground powder was dispersed in ethanol, and the powder sample was separated on the basis of the falling time corresponding to the size between a few micrometer and $\sim 10 \mu\text{m}$, which are calculated using the Stokes's law without taking into account the Brownian motion. The separated powder sample was annealed with a carbon buffer at 700°C for 2 h in vacuum to relieve internal stress.

The strong-field thermomagnetic curve of the annealed sample was measured in a field of 500 mT between 50 and 700°C in a helium gas flow using a MicroMag 3900 vibrating sample magnetometer (VSM, Princeton Measurements Corporation). The strong-field thermomagnetic curve shows a single Curie temperature of 572°C (Figure 1a), indicating the Curie temperature of stoichiometric magnetite [Dunlop and Özdemir, 1997, Table 3.1]. A series of low-temperature remanence curves of the annealed sample was measured between 10 and 300 K using the MPMS (Figure 1b). The sample was cooled in zero field from 300 to 10 K and an isothermal remanent magnetization (IRM) was imparted for the sample in a field of 2.5 T (ZFC remanence). A thermal demagnetization curve of the ZFC remanence was measured during zero-field warming (ZFW) from 10 to 300 K. Subsequently, the sample was cooled from 300 to 10 K in a field of 2.5 T (FC remanence) and a thermal demagnetization curve of the FC remanence was measured during ZFW from 10 to 300 K. Lastly, a saturation IRM (SIRM) was imparted for the sample in a field of 2.5 T at 300 K (RT-SIRM) and a demagnetization curve of the RT-SIRM was measured during low-temperature demagnetization (LTD) cycle between 10 and 300 K. The ZFC remanence and FC remanence were sharply demagnetized at approximately 120 K during ZFW from 10 to 300 K, and RT-SIRM was significantly demagnetized at approximately 120 K during the LTD cycle, indicating the Verwey transition of stoichiometric magnetite [Moskowitz *et al.*, 1998; Özdemir *et al.*, 1993].

The grain size and shape of the annealed sample were observed for 250 grains using a field emission scanning electron microscope (FE-SEM, JEOL). The grain size distribution of the annealed sample is shown in Figure 1c. The grain size varied from 0.13 to 7.24 μm with the arithmetic mean of 0.93 μm and the volume weighted arithmetic mean of 4.92 μm . The observed maximum grain size is consistent with the falling time in the ethanol, while the minimum is smaller than that expected from the falling time. The difference arose from the adhering of small grains in large grain and the aggregation of small grains during the separation. The average aspect ratio of the sample was 1.50. The magnetic hysteresis parameters (B_c , saturation remanence M_{rs} , saturation magnetization M_s , and coercivity of remanence B_{cr}) of the annealed sample were measured using the VSM. The ratios of hysteresis parameters (M_{rs}/M_s and B_{cr}/B_c) were plotted near the PSD/MD boundary over the Day plot [Day *et al.*, 1977], and the annealed sample slightly deviates away from the SD-MD mixing line in Dunlop [2002] (Figure 1d). The deviation may result from the grain size distribution from 0.13 to 7.24 μm ; the B_{cr}/B_c for the mixed phase is sometime larger than that for end-members [Dunlop, 2002].

The relationship between the grain size and B_c is shown in Figure 1e. The annealed sample results in the relationship consistent with the trend of low-stress magnetites [Heider *et al.*, 1987]. The grain size of the

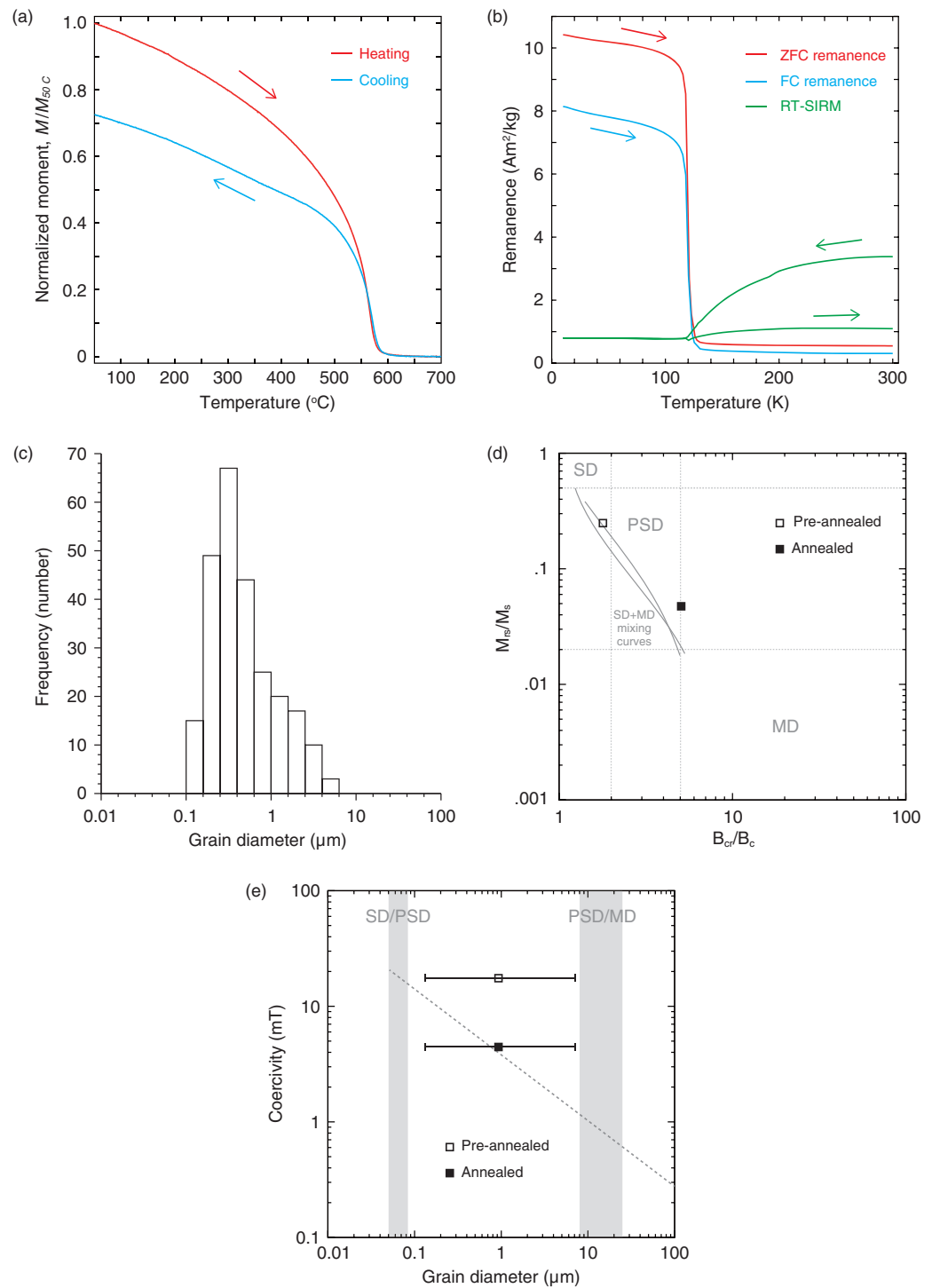


Figure 1. Rock-magnetic data of the BZ4 sample. (a) Strong-field thermomagnetic curve. Arrows indicate heating and cooling directions. (b) Low-temperature remanence curves. Arrows indicate warming and cooling directions. (c) Grain size distribution. (d) Day plot. Threshold values for SD/PSD and PSD/MD are shown as dashed lines [Dunlop, 2002]. The SD-MD mixing lines in Dunlop [2002] are also shown as gray lines. (e) The relationship between grain diameter and coercivity. The arithmetic mean and range of the grain size are shown as the black square and line, respectively. The dashed line indicates the trend for low-stress magnetites [Heider et al., 1987]. The threshold grain sizes for SD/PSD [Dunlop and Özdemir, 1997, Table 5.1] and PSD/MD [e.g., Dankers and Sugiura, 1981; Moskowitz and Banerjee, 1979] are shown as a guide.

annealed sample was greater than the SD/PSD thresholds [Dunlop and Özdemir, 1997, Table 5.1]. Although the grain size of the PSD/MD threshold is not very clear, the grain size of the annealed sample was sufficiently smaller than the PSD/MD threshold [e.g., Dankers and Sugiura, 1981; Moskowitz and Banerjee, 1979].

In the low-temperature remanence measurements, the intensity of ZFC remanence was slightly greater than that of FC remanence at 10 K (Figure 1b); $J_{ZFC}(10)/J_{FC}(10) = 1.28$, where $J_{ZFC}(T)$ and $J_{FC}(T)$ are intensities of ZFC remanence and FC remanence at temperature T , respectively. This behavior is intermediate between SD magnetite ($J_{ZFC}(10)/J_{FC}(10) = 0.66$ [Sato *et al.*, 2015]) and MD magnetites ($J_{ZFC}(10)/J_{FC}(10) = 2.03$ [Sato *et al.*, 2014]) used in the previous studies. The δ_{FC} and δ_{ZFC} values are 0.95 and 0.94 and the ratio δ_{ZFC}/δ_{FC} is 1.0, where δ_{FC} and δ_{ZFC} are defined as $\delta_{FC} = \{J_{FC}(80) - J_{FC}(150)\}/J_{FC}(80)$ and $\delta_{ZFC} = \{J_{ZFC}(80) - J_{ZFC}(150)\}/J_{ZFC}(80)$, respectively [Moskowitz *et al.*, 1993]. The δ_{FC} and δ_{ZFC} values are slightly larger than those of the sized magnetite sample with mean dimension of 1000 nm in Moskowitz *et al.* [1993]. The RT-SIRM curves reduced to $\sim 30\%$ of the original RT-SIRM intensity at 300 K after the LTD cycle, which is consistent with the LTD memory of SIRM of the low-stress magnetite with $\sim 1 \mu\text{m}$ grain size [Heider *et al.*, 1992]. These results indicate that the annealed sample is a stoichiometric magnetite with a PSD grain size.

To minimize sample geometry deformation, which affects magnetic hysteresis curves owing to a change in the demagnetizing factor, the annealed sample powder was mixed with a silicone adhesive, and we prepared two cylindrical specimens of 2 mm in diameter and 1.6 mm in height (BZ4-A and BZ4-B).

3. High-Pressure Experiment

We followed the method of magnetic measurements under high pressure by Sato *et al.* [2014], and the magnetic measurements were carried out using the MPMS and the piston-cylinder high-pressure cell made of BeCu and zirconium oxide (ZrO_2) [Sato *et al.*, 2012, 2014, 2015]. A Teflon capsule and disc were placed inside the high-pressure cell. The Teflon capsule was composed of a small chip of indium, a resin cylinder, glass wool, the cylindrical specimen, and a liquid pressure-transmitting medium (1:1 mixture of Fluorinert No. FC70 and No. FC77).

A hydrostatic pressure condition was evaluated using the superconducting transition temperature of indium (~ 3 K) and the transition temperature of magnetite. Changes in the superconducting transition temperatures of indium were used to calculate the pressure values [Jennings and Swenson, 1958]. The transition temperature of indium was determined with precision of 0.005 K in our method, and the uncertainty of pressure determination due to the uncertainty of transition temperature determination is estimated to be < 0.015 GPa in the < 1 GPa pressure range. The pressure differences between about 3 and 300 K were evaluated by the Curie temperature measurement of gadolinium (~ 295 K at 0 GPa), which is also known as a function of pressure [McWhan and Stevens, 1965], indicating that the pressure differences between about 3 and 300 K are smaller than 0.06 GPa in the > 0.5 GPa range [Sato *et al.*, 2015]. Changes in the demagnetization temperature (T_d) were used to evaluate the hydrostatic condition (see section 5.1). The T_d was defined as a median demagnetization temperature of ZFC remanence between 20 and 150 K [Sato *et al.*, 2014], i.e., $\{J_{ZFC}(T_d) - J_{ZFC}(150)\}/\{J_{ZFC}(20) - J_{ZFC}(150)\} = 0.5$.

One measurement cycle consisted of (1) the transition temperature measurement of indium, (2) the thermal demagnetization curve measurement of ZFC remanence imparted in a 2.5 T field at 20 K, (3) the magnetic hysteresis loop measurement at 300 K, and (4) the direct field demagnetization curve measurement of SIRM at 300 K. In the hysteresis loop measurement, the maximum field was 700 mT, about two times the saturation field of magnetite, and a field increment of 4 mT (10 or 50 mT) was set when the applied field was close to zero (in other cases). In the direct field demagnetization curve measurement, the sample remanence was measured with 4 mT steps.

In addition to the high-pressure experiments of the BZ4 samples, the hysteresis curves of a pure silicone adhesive specimen of cylindrical form were measured in the same manner as those of the BZ4 samples at atmospheric pressure to evaluate a background level. The magnetic hysteresis curves of the BZ4 samples were also measured using the VSM before and after the high-pressure experiment to evaluate the effect of high-pressure experiments on the samples.

4. Results

The magnetic hysteresis loops of the BZ4 samples as well as the pure silicone adhesive specimen (background curve) are shown in Figures 2a–2d. The background curve shows a weak diamagnetic character, and hysteresis characteristic of the background curve is negligible relative to those of the BZ4 samples. Thus, we made only slope corrections to the BZ4 loops by subtracting the diamagnetic/paramagnetic slopes

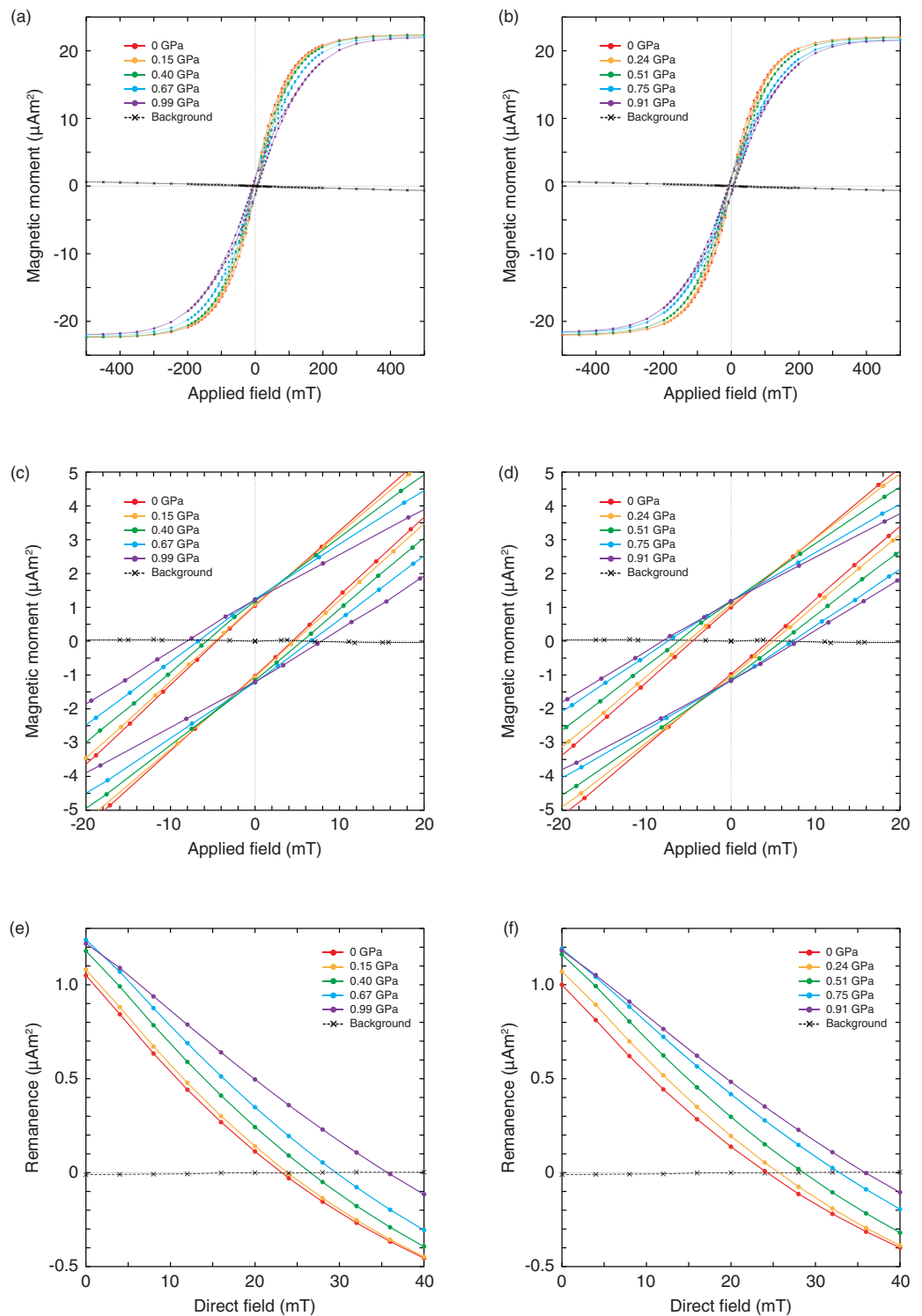


Figure 2. Magnetic measurement curves of (a, c, e) BZ4-A and (b, d, f) BZ4-B are plotted together with the background curves. The hysteresis loops of BZ4 samples are corrected by subtracting diamagnetic/paramagnetic slopes at the $|B| > 400$ mT range. (a, b) Magnetic hysteresis loops. (c, d) Extended view of the loops. (e, f) Direct field demagnetization curves.

in $|B| > 400$ mT ranges. The corrected hysteresis loops change with increasing pressure: total susceptibilities decrease with increasing pressure (Figures 2a and 2b), and they become magnetically hard under high pressure (Figures 2c and 2d). The direct field demagnetization curves of SIRM change with increasing pressure (Figures 2e and 2f).

Table 1. Summary of the High-Pressure Experiment

| Sample | Apparatus | P (GPa) | B _c (mT) | M _{rs} (μAm ²) | M _s (μAm ²) | B _{cr} (mT) | M _{rs} /M _s (×10 ⁻²) | B _{cr} /B _c | T _d (K) |
|--|-----------|---------|---------------------|-------------------------------------|------------------------------------|----------------------|--|---------------------------------|--------------------|
| BZ4-A | MPMS | 0 | 4.47 | 1.04 | 22.3 | 23.2 | 4.66 | 5.18 | 120.6 |
| | | 0.15 | 4.69 | 1.07 | 22.3 | 23.8 | 4.83 | 5.08 | 120.1 |
| | | 0.40 | 5.66 | 1.17 | 22.3 | 26.6 | 5.26 | 4.69 | 119.5 |
| | | 0.67 | 6.65 | 1.23 | 22.1 | 29.6 | 5.58 | 4.46 | 118.8 |
| | | 0.99 | 7.96 | 1.22 | 21.9 | 35.7 | 5.56 | 4.49 | 118.5 |
| BZ4-A before pressurization | VSM | | 4.36 | 1.08 | 21.9 | 21.7 | 4.91 | 4.99 | |
| BZ4-A after pressurization and decompression | VSM | | 4.54 | 1.05 | 21.6 | 21.8 | 4.89 | 4.81 | |
| BZ4-B | MPMS | 0 | 4.53 | 0.99 | 22.0 | 24.2 | 4.50 | 5.35 | 120.6 |
| | | 0.24 | 5.07 | 1.07 | 22.0 | 25.6 | 4.85 | 5.06 | 119.5 |
| | | 0.51 | 6.13 | 1.15 | 21.9 | 28.6 | 5.28 | 4.66 | 119.0 |
| | | 0.75 | 7.38 | 1.18 | 21.6 | 32.8 | 5.46 | 4.44 | 118.7 |
| | | 0.91 | 8.04 | 1.18 | 21.5 | 35.8 | 5.48 | 4.46 | 118.2 |
| BZ4-B before pressurization | VSM | | 4.53 | 0.98 | 21.6 | 23.3 | 4.56 | 5.13 | |
| BZ4-B after pressurization and decompression | VSM | | 4.62 | 1.03 | 20.8 | 22.4 | 4.98 | 4.85 | |

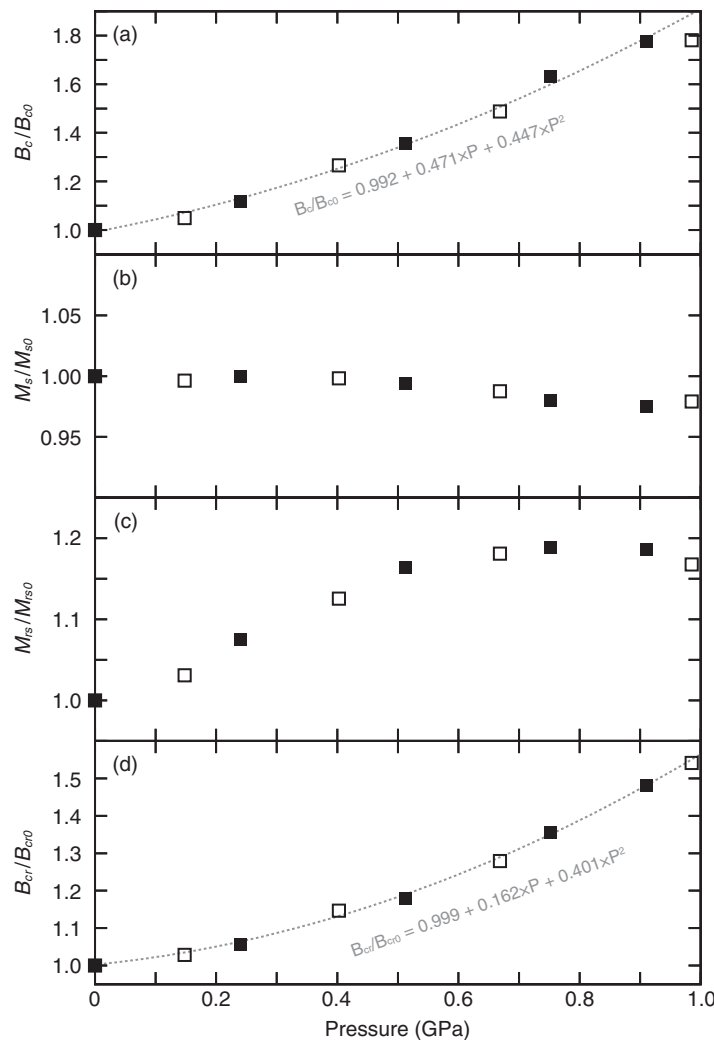


Figure 3. Pressure effect on the normalized magnetic hysteresis parameters. $B_c(P)/B_{c0}$, $M_s(P)/M_{s0}$, $M_{rs}(P)/M_{rs0}$, and $B_{cr}(P)/B_{cr0}$, where $X(P)$ represents a hysteresis parameter at pressure P and X_0 represents that for an untreated sample (equivalent to $X(0)$). The results for BZ4-A and BZ4-B are shown by open and closed squares, respectively. (a) Coercivity, $B_c(P)/B_{c0}$. (b) Saturation magnetization, $M_s(P)/M_{s0}$. (c) Saturation remanent magnetization, $M_{rs}(P)/M_{rs0}$. (d) Coercivity of remanence, $B_{cr}(P)/B_{cr0}$. The dotted lines in Figures 3a and 3d indicate the pressure dependence equations. The BZ4-A data points at 0.99 GPa are excluded from the pressure dependence calculations (see text).

The magnetic hysteresis parameters of the BZ4 samples at each pressure level were calculated from the magnetic hysteresis loops and direct field demagnetization curves of SIRM (Table 1). The hysteresis parameters measured using the high-pressure apparatus at atmospheric pressure agree well with those of the VSM measurements (Table 1), guaranteeing the results of high-pressure experiment. The magnetic hysteresis parameters of the BZ4 samples before and after the high-pressure experiment are similar to each other (Table 1), indicating elastic behavior in the <1 GPa pressure range. This elastic behavior is consistent with the previous study; *Bezaeva et al.* [2010] reported that the application of ~1.2 GPa do not permanently change the hysteresis properties of PSD magnetite.

The normalized magnetic hysteresis parameters, where a parameter at pressure is divided by that of an untreated sample, are plotted as a function of pressure in Figure 3. The pressure dependences of the normalized hysteresis parameters of BZ4-A and BZ4-B are consistent. The normalized B_c does not increase linearly but as a

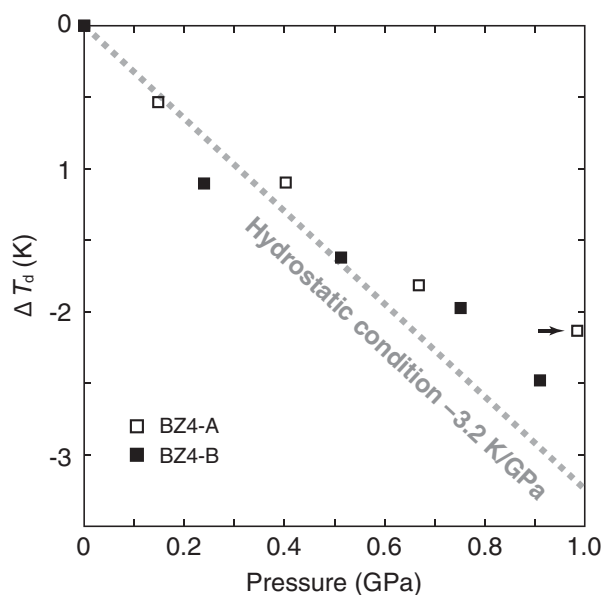


Figure 4. Relative changes in T_d are plotted as a function of pressure. The results for BZ4-A and BZ4-B are shown by open and closed squares, respectively. The dashed line indicates the slope for the hydrostatic condition [Sato *et al.*, 2014]. The arrow indicates the anomalous point, which is excluded from the pressure dependence calculation.

quadratic function (Figure 3a), which is different from those of MD [Sato *et al.*, 2014] and SD magnetites [Sato *et al.*, 2015] (see section 5.2). The change in M_s is within 3% in the <1 GPa pressure range (Figure 3b), which is in good agreement with the results of MD [Sato *et al.*, 2014] and SD magnetites [Sato *et al.*, 2015]. The normalized M_{rs} increases with pressure and then appears to reach saturation at about 0.5 GPa (Figure 3c). This saturation is also observed in MD magnetite [Sato *et al.*, 2014]. The normalized B_{cr} increases as a quadratic function (Figure 3d).

Relative changes in the T_d are plotted as a function of pressure in Figure 4. It is clearly seen that the T_d of BZ4-A and BZ4-B samples decrease with increasing pressure. Except for the BZ4-A data point at 0.99 GPa, the relative changes in T_d of BZ4-A and BZ4-B samples are consistent; this result is similar to the normalized hysteresis parameters.

5. Discussion

5.1. Hydrostatic Pressure Condition

The pressure dependence of the Verwey transition temperature, which is the structural transition from cubic to monoclinic symmetry of magnetite at approximately 120 K [Verwey, 1939; Walz, 2002, and references therein], varies from negative to positive depending on the degree of nonhydrostatic stress [Coe *et al.*, 2012]. Sato *et al.* [2014] proposed that change in T_d , which is equivalent to change in the Verwey transition temperature [Sato *et al.*, 2012], could be used as a barometer for the hydrostatic condition. Using MD magnetite samples, Sato *et al.* [2014] reported the slope for the hydrostatic condition (-3.2 K/GPa). Since the structural phase transition temperature may not be affected by grain size of magnetite, it is reasonable to consider that the hydrostatic pressure dependence value of T_d measured using MD magnetite is equivalent to that of PSD magnetite. The relative changes in T_d for the BZ4 samples agree well with the hydrostatic reference line of MD magnetite, except for the BZ4-A data point at 0.99 GPa (Figure 4). Thus, we excluded this anomalous point from the calculations for the hydrostatic pressure dependence of the magnetic properties of PSD magnetite.

5.2. Pressure Dependences of Coercivity for SD, PSD, and MD Magnetite

The pressure dependences of B_c of SD, PSD, and MD magnetites are summarized in Figure 5. In this study, B_c of PSD magnetite increases with increasing pressure as a quadratic function, and its calculated pressure dependence is

$$B_c(P)/B_{c0} = 0.992 + 0.471 \times P/\text{GPa} + 0.447 \times (P/\text{GPa})^2, \quad (1)$$

where $B_c(P)$ and B_{c0} are B_c at pressure P and at atmospheric pressure, respectively. The pressure dependence of B_c of PSD magnetite is clearly different from those of MD and SD magnetites reported in previous experimental studies [Sato *et al.*, 2014, 2015]. Using the same apparatus as used in this study, in situ magnetic hysteresis measurement under high pressures of MD [Sato *et al.*, 2014] and SD magnetites [Sato *et al.*, 2015] were conducted. In the case of MD magnetite, B_c linearly increased with increasing pressure [Sato *et al.*, 2014]

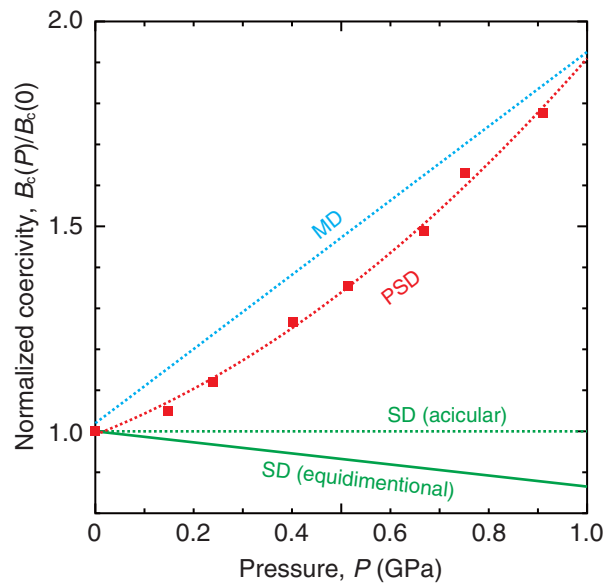


Figure 5. Summary of the pressure dependence of coercivity. The results for BZ4 samples are shown by squares. The lines indicate the pressure dependence equations (see text).

$$B_c(P)B_{c0}=1.02+0.91\times P/\text{GPa}. \quad (2)$$

In the case of SD magnetite, B_c was almost constant up to 1 GPa within the experimental error [Sato *et al.*, 2015]; the result was consistent with theoretical estimation. The pressure effects on B_c of SD magnetite change depending on the mechanism dominating the magnetic property, i.e., magnetite grain shape. As the aspect ratio of a magnetite grain is unaffected by hydrostatic compression, the B_c of acicular-SD magnetite (shape anisotropy dominating) is expected to be constant under high pressure

$$B_c(P)/B_{c0}=1. \quad (3)$$

In the case of equidimensional SD magnetite (magnetic anisotropy dominating), B_c is expected to decrease with increasing pressure due to the decrease in magnetic anisotropy constant [Sawaoka and Kawai, 1968]

$$B_c(P)/B_{c0}=1-0.135\times P/\text{GPa}. \quad (4)$$

In the case of PSD and MD magnetites, the magnetic properties remain to be theoretically understood. Thus, empirical equations (1) and (2) deduced from the experimental observations are useful for estimating the B_c values of PSD and MD magnetites under condition similar to the high pressure in the deep crust. Note that this study investigated on the PSD magnetite with mean grain size of $\sim 1 \mu\text{m}$ and size distribution from 0.13 to 7.24 μm , and thus the data for coarse-grained PSD magnetite ($\sim 10 \mu\text{m}$), fine-grained PSD magnetite ($< \sim 1 \mu\text{m}$), and narrowly sized PSD magnetite samples should be investigated in the future study, to understand the behavior of whole PSD family.

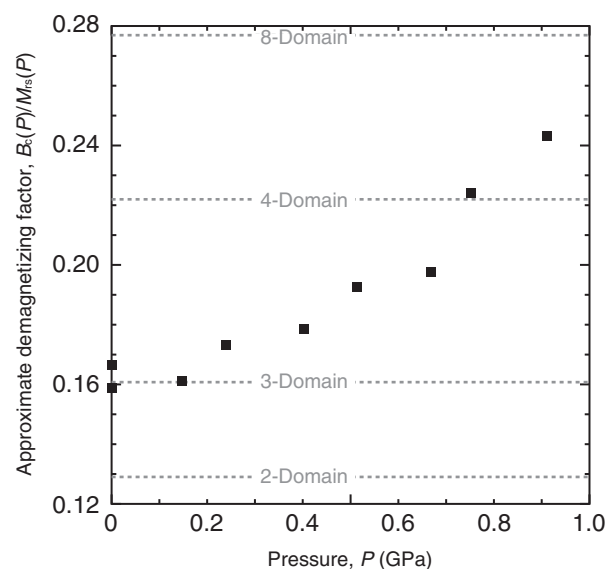


Figure 6. Pressure dependence of approximate demagnetizing factor calculated from saturation remanence and coercivity. The dashed line indicates the theoretical demagnetizing factor for lamellar n -domain grains [Dunlop, 1983].

5.3. Magnetic Domain Structure Under High Pressure

An approximate value of the average demagnetizing factor can be calculated from the ratio B_c/M_{rs} [Argyle and Dunlop, 1990]. Figure 6 shows the pressure dependence of the approximate demagnetizing factor calculated from the results obtained in this study, together with the theoretical demagnetizing factors for lamellar two, three, four, and eight-domain structures in a magnetite cube [Dunlop, 1983]. The approximate demagnetizing factor increases with increasing pressure, suggesting that the number of lamellar domains increases with increasing pressure.

The increase in the number of lamellar domains could be caused by the pressure effect on the magnetic anisotropic energy and magnetoelastic energy. To minimize

the sum of exchange energy and magnetocrystalline anisotropy energy in a domain wall, the domain wall width δ_w and domain wall energy per unit area γ_w at equilibrium are given by

$$\delta_w = \pi \left(\frac{A}{K} \right)^{\frac{1}{2}} \propto K^{-\frac{1}{2}} \quad (5)$$

and

$$\gamma_w = 2\pi(AK)^{\frac{1}{2}} \propto K^{\frac{1}{2}}, \quad (6)$$

where A and K are the exchange constant and magnetocrystalline anisotropy energy per unit volume, respectively [Dunlop and Özdemir, 1997, equations (5.10) and (5.11)]. The pressure dependences of the magnetocrystalline anisotropy constant K_1 of Fe_3O_4 has been reported to be $-13.5\%/GPa$ [Sawaoka and Kawai, 1968]. Thus, δ_w (γ_w) increases (decreases) with increasing pressure because of the decrease in the magnetocrystalline anisotropy energy. Substituting the pressure dependences of K_1 into equation (5), the domain wall width at 1 GPa normalized by that at ambient pressure is estimated to be $\delta_w(1 \text{ GPa})/\delta_w(0 \text{ GPa}) \sim 1.08$. In the case of a magnetite cube with lamellar and closure domains, the number of lamellar domains n to minimize the sum of magnetoelastic energy and domain wall energy is given by

$$n = \left(\frac{9\lambda_{111}^2 c_{44}}{4\gamma_w} \right)^{1/2} L^{1/2}, \quad (7)$$

where λ_{111} , c_{44} , and L are the magnetostriction constant, elastic constant, and magnetite cube length, respectively [Dunlop and Özdemir, 1997, equation (5.23)]. Substituting equation (6) into equation (7), the number of lamellar domains n is expressed as

$$n = \left(\frac{9\lambda_{111}^2 c_{44}}{8\pi A^{\frac{1}{2}} K^{\frac{3}{2}}} \right)^{\frac{1}{2}} L^{\frac{1}{2}} \propto \lambda_{111}^{\frac{1}{2}} c_{44}^{\frac{1}{2}} K^{-\frac{1}{4}}. \quad (8)$$

The pressure dependences of λ_{111} and c_{44} of magnetite have been reported to be $150\%/GPa$ [Nagata and Kinoshita, 1967] and $-0.205\%/GPa$ [Reichmann and Jacobsen, 2004], respectively. Substituting the pressure dependences of λ_{111} , c_{44} , and K_1 into equation (8), the number of lamellar domains is expected to increase with increasing pressure: the number of lamellar domains at 1 GPa normalized by that at ambient pressure is estimated to be $n(1 \text{ GPa})/n(0 \text{ GPa}) \sim 2.59$. The increase in the number of lamellar domains is consistent with the increase in the approximate demagnetizing factor calculated from the magnetic hysteresis parameters. Boyd *et al.* [1984] conducted the magnetic domain observation on a magnetite particle of IRM state during stress cycling to a few hundred bars. They found that magnetic domain walls were nucleated with the application of stress and the domain pattern rearranged to give a lower energy and that the domain numbers decreased irreversibly to give typical body domain after the stress was reduced to zero. The observation that domain number increased under stress state further supports the above estimation. Although the detailed magnetic domain structure under high pressure should be investigated using micromagnetic calculations in a future study, the increases in the number of lamellar domains and/or domain wall width are expected to occur under high pressure and these changes should relate to the changes in the magnetic properties of PSD magnetite.

6. Conclusions

To investigate hydrostatic pressure effects on the magnetic hysteresis parameters of PSD magnetite, we have conducted in situ magnetic hysteresis measurements of PSD magnetite under high pressures up to 1 GPa. The stoichiometric magnetite with PSD grain size, which is carefully characterized by the rock magnetic measurements and microscopic observation, was used as the experimental samples. The magnetic hysteresis loop and direct field demagnetization curve of SIRM at 300 K and under high pressure were measured using the high-pressure cell specially designed for the MPMS, which enabled us to directly measure the magnetic hysteresis curves with high precision. The hydrostatic pressure condition was evaluated from the change in transition temperature of magnetite. The pressure effects on the magnetic hysteresis parameters of PSD magnetite are (1) B_c and B_{cr} increase with increasing pressure as a quadratic function, (2) M_s is almost constant, and (3) M_{rs} increases with increasing pressure up to 0.5 GPa and then appears to reach saturation.

The approximate demagnetizing factor calculated from the ratio B_c/M_{rs} increases with increasing pressure, suggesting that the number of lamellar domains increases with increasing pressure. Considering the pressure dependences of the magnetostriction, elastic, and magnetocrystalline anisotropy constants, the number of lamellar domains is theoretically estimated to increase with increasing pressure, which is consistent with our experimental results. The magnetic domain wall width is also expected to increase with increasing pressure, and these changes in magnetic domain structure should closely relate to the changes in the magnetic properties of PSD magnetite.

Acknowledgments

This study was performed under the cooperative research program of Center for Advanced Marine Core Research (CMCR), Kochi University (Accept 10A017, 10B017, 11A016, 11B014, 12A027, and 12B024). This research was supported by grant for the Global COE Program "From the Earth to "Earths," from the Ministry of Education, Culture, Sports, Science and Technology of Japan. Data from this paper can be accessed through the corresponding author. We thank the three anonymous reviewers for their thoughtful and thorough reviews of the manuscript.

References

- Argyle, K. S., and D. J. Dunlop (1990), Low-temperature and high-temperature hysteresis of small multidomain magnetites, *J. Geophys. Res.*, *95*, 7069–7083.
- Bezaeva, N. S., J. Gattacceca, P. Rochette, R. A. Sadykov, and V. I. Trukhin (2010), Demagnetization of terrestrial and extraterrestrial rocks under hydrostatic pressure up to 1.2 GPa, *Phys. Earth Planet. Inter.*, *179*, 7–20.
- Boyd, J. R., M. Fuller, and S. Halgedahl (1984), Domain wall nucleation as a controlling factor in the behaviour of fine magnetic particles in rocks, *Geophys. Res. Lett.*, *11*, 193–196.
- Carmichael, R. S. (1969), Hydrostatic pressurization of magnetite, *Geophysics*, *34*, 775–779.
- Coe, R. S., R. Egli, S. A. Gilder, and J. P. Wright (2012), The thermodynamic effect of nonhydrostatic stress on the Verwey transition, *Earth Planet. Sci. Lett.*, *319–320*, 207–217.
- Dankers, P., and N. Sugiura (1981), The effect of annealing and concentration on the hysteresis properties of magnetite around the PSD-MD transition, *Earth Planet. Sci. Lett.*, *56*, 422–428.
- Day, R., M. Fuller, and V. A. Schmidt (1977), Hysteresis properties of titanomagnetites: Grain-size and compositional dependence, *Phys. Earth Planet. Inter.*, *13*, 260–267.
- Dunlop, D. J. (1983), On the demagnetizing energy and demagnetizing factor of a multidomain ferromagnetic cube, *Geophys. Res. Lett.*, *10*, 79–82.
- Dunlop, D. J. (2002), Theory and application of the Day plot (M_r/M_s versus H_c/H_s): 1. Theoretical curves and tests using titanomagnetite data, *J. Geophys. Res.*, *107*(B3), 1–22, doi:10.1029/2001JB000486.
- Dunlop, D. J., and Ö. Özdemir (1997), Rock magnetism: Fundamentals and frontiers, in *Cambridge Studies in Magnetism*, vol. 3, 573 pp., Cambridge Univ. Press, Cambridge, U. K.
- Gilder, S. A., and M. LeGoff (2008), Systematic pressure enhancement of titanomagnetite magnetization, *Geophys. Res. Lett.*, *35*, L10302, doi:10.1029/2008GL033325.
- Gilder, S. A., M. LeGoff, J. Peyronneau, and J. Chervin (2002), Novel high pressure magnetic measurements with application to magnetite, *Geophys. Res. Lett.*, *29*(10), 1392, doi:10.1029/2001GL014227.
- Gilder, S. A., M. LeGoff, J. Chervin, and J. Peyronneau (2004), Magnetic properties of single and multi-domain magnetite under pressures from 0 to 6 GPa, *Geophys. Res. Lett.*, *31*, L10612, doi:10.1029/2004GL019844.
- Heider, F., D. J. Dunlop, and N. Sugiura (1987), Magnetic properties of hydrothermally recrystallized magnetite crystals, *Science*, *236*, 1287–1290.
- Heider, F., D. J. Dunlop, and H. C. Soffel (1992), Low-temperature and alternating field demagnetization of saturation remanence and thermoremanence in magnetite grains (0.037 μm to 5 mm), *J. Geophys. Res.*, *97*, 9371–9381.
- Jennings, L. D., and C. A. Swenson (1958), Effects of pressure on the superconducting transition temperatures of Sn, In, Ta, Tl, and Hg, *Phys. Rev.*, *112*, 31–43.
- Jiang, Z., P. Rochette, Q. Liu, J. Gattacceca, Y. Yu, V. Barrón, and J. Torrent (2013), Pressure demagnetization of synthetic Al substituted hematite and its implications for planetary studies, *Phys. Earth Planet. Inter.*, *224*, 1–10.
- McWhan, D. B., and A. L. Stevens (1965), Effect of pressure on the magnetic properties and crystal structure of Gd, Tb, Dy, and Ho, *Phys. Rev.*, *139*, A682–A689.
- Moskowitz, B. M., and S. K. Banerjee (1979), Grain size limits for pseudosingle domain behavior in magnetite: Implications for paleomagnetism, *IEEE Trans. Magn.*, *MAG-15*, 1241–1246.
- Moskowitz, B. M., R. B. Frankel, and D. A. Bazylinski (1993), Rock magnetic criteria for the detection of biogenic magnetite, *Earth Planet. Sci. Lett.*, *120*, 283–300.
- Moskowitz, B. M., M. Jackson, and C. Kissel (1998) Low-temperature magnetic behavior of titanomagnetites, *Earth Planet. Sci. Lett.*, *157*, 141–149.
- Nagata, T., and H. Kinoshita (1967), Effect of hydrostatic pressure on magnetostriction and magnetocrystalline anisotropy of magnetite, *Phys. Earth Planet. Inter.*, *1*, 44–48.
- Özdemir, Ö., D. J. Dunlop, and B. M. Moskowitz (1993), The effect of oxidation on the Verwey transition in magnetite, *Geophys. Res. Lett.*, *20*, 1671–1674.
- Reichmann, H. J., and S. D. Jacobsen (2004), High-pressure elasticity of a natural magnetite crystal, *Am. Mineral.*, *89*, 1061–1066.
- Sato, M., Y. Yamamoto, T. Nishioka, K. Kodama, N. Mochizuki, and H. Tsunakawa (2012), Pressure effect on low-temperature remanence of multidomain magnetite: change in demagnetization temperature, *Geophys. Res. Lett.*, *39*, L04305, doi:10.1029/2011GL050402.
- Sato, M., Y. Yamamoto, T. Nishioka, K. Kodama, N. Mochizuki, and H. Tsunakawa (2014), Hydrostatic pressure effect on magnetic hysteresis parameters of multidomain magnetite: Implication for crustal magnetization, *Phys. Earth Planet. Inter.*, *233*, 33–40.
- Sato, M., Y. Yamamoto, T. Nishioka, K. Kodama, N. Mochizuki, Y. Usui, and H. Tsunakawa (2015), Pressure effect on magnetic hysteresis parameters of single-domain magnetite contained in natural plagioclase crystal, *Geophys. J. Int.*, *202*, 394–401.
- Sawaoka, A., and N. Kawai (1968), The effect of hydrostatic pressure on the magnetic anisotropy of ferrous and ferric ions in ferrites with spinel structure, *J. Phys. Soc. Jpn.*, *25*, 133–140.
- Verwey, E. J. W. (1939), Electric conduction of magnetite (Fe_3O_4) and its transition point at low temperatures, *Nature*, *144*, 327–328.
- Walz, F. (2002), The Verwey transition—A topical review, *J. Phys. Condens. Matter*, *14*, R285–R340.
- Wasilewski, P. J., and M. A. Mayhew (1992), The Moho as a magnetic boundary revisited, *Geophys. Res. Lett.*, *19*, 2259–2262.